JOURNAL OF SOLID STATE CHEMISTRY **139,** 274–280 (1998)
ARTICLE NO. SC987841

Synthesis and Crystal Structure of $Bi_{6.67}(PO_4)_4O_4$ Oxyphosphate: The $Bi_6M^{2+}(PO_4)_4O_4$ and $Bi_{6.5}A^{+}_{0.5}(PO_4)_4O_4$ Series

Mustafa Ketatni,[1] Olivier Mentre,[2] and Francis Abraham

Laboratoire de Cristallochimie et Physicochimie du Solide URA, CNRS 452, ENSCL, Université des Sciences et Technologies de Lille, BP 108, 59652 Villeneuve d'Ascq Cedex, France

and

Fouzia Kzaiber[1] and Bouchaïb Mernari

Laboratoire de Physicochimie des Matériaux, Faculté des Sciences, Université Chouaïb Doukkali, BP 20, El Jadida, Morocco

Received December 18, 1997; in revised form March 31, 1998; accepted April 5, 1998

Single crystals of a new bismuth oxyphosphate were isolated and X-ray investigated, leading to the formula $Bi_{6.67}(PO_4)_4O_4$. Its crystal structure was refined using 2624 independent reflections in the $P\bar{1}$ space group, $a = 9.195(15)$ Å, $b = 7.552(5)$ Å, $c = 6.933(4)$ Å, $\alpha = 112.2(1)^\circ$, $\beta = 93.9(1)^\circ$, $\gamma = 106.9(1)^\circ$, $Z = 1$, with the final $R = 0.049$, $R_w = 0.060$. It consists of infinite chains running parallel to the a axis formed by the linkage of BiO_5, BiO_6, and BiO_8 polyhedra. These chains are connected by BiO_8 polyhedra, in which the central atom partially occupies the 1(a) inversion center. That produces $(Bi_{6.67}O_{20})^{20-}_{\infty}$ slabs parallel to the (ac) plane. Finally, the cohesion between the layers is provided by the interconnection of PO_4^{3-} species. This phase was previously evidenced during the Bi_2O_3–$BiPO_4$ phase diagram study and behaves on cooling as an incongruently melting compound stable above 910°C. It was therefore assigned to the $2Bi_2O_3$–$7BiPO_4$ composition very close to our corresponding $2Bi_2O_3$–$6BiPO_4$ ($Bi_{6.67}P_4O_{20}$) revised stoichiometry. Pure polycrystalline samples were room temperature stabilized by substitution of several cations for a substantial part of bismuth. This yielded the new series $Bi_6MP_4O_{20}$ ($M = Sr^{2+}$, Cd^{2+}, Ca^{2+}, Pb^{2+}) and $Bi_{6.5}A_{0.5}P_4O_{20}$ ($A = Li^+$, Na^+, K^+) presented in the aforementioned phase diagram study. The substitution involves only the bismuth atom labeled Bi(4) because of its peculiar role within the framework. © 1998 Academic Press

INTRODUCTION

The Bi_2O_3–$BiPO_4$ system was recently reinvestigated (1), completing the previous study of Volkov *et al.* (2). At room temperature, four compounds were identified with the $Bi_2O_3 : BiPO_4$ ratios 11:9, 12:13, 1:2, and 3:8. In addition, three high-temperature compounds were identified. $1Bi_2O_3$–$1BiPO_4$ (Bi_3PO_7) decomposes below 890°C into $11Bi_2O_3$–$9BiPO_4$ and $5Bi_2O_3$–$7BiPO_4$ phases, the latter being stable only in a narrow thermal range and producing $12Bi_2O_3$–$13BiPO_4$ and $1Bi_2O_3$–$2BiPO_4$ on cooling. Finally, $2Bi_2O_3$–$7BiPO_4$ is observed only above 910°C. Neither of these was structurally characterized. Only the sillenite-type solid solution in the Bi_2O_3-rich part of the diagram was extensively studied (3, 4), particularly for its electrical properties. Moreover, substitution of V for P improves oxygen conductivity in the Bi_7PO_{13} compound which adopts a superstructure of the δ-Bi_2O_3 fcc form (5). On the other hand, the discovery of high ionic conductivity in BIMEVOX derivates of $Bi_4V_2O_{11}$ (6–10) has generated the reinvestigation of several Bi_2O_3–V_2O_5–M_xO_y and Bi_2O_3–P_2O_5–M_xO_y systems (11, 12). It is well known that impurities or mineralizer can stabilize high-temperature phases under ambient conditions. For example, during the study of the Bi_2O_3–P_2O_5–NiO ternary diagram, Bi_3PO_7 was found to be stabilized at room temperature by nickel impurities (11). In the same way, during investigation of the Bi_2O_3–P_2O_5–CoO system, single crystals of the previously formulated $2Bi_2O_3$–$7BiPO_4$ high-temperature phase were obtained. This paper reports the crystal structure determination of this compound and the preparation of isotypic compounds obtained by substitution of some peculiar bismuth by monovalent or divalent cations, including Pb^{2+}, and leading to the new $PbBi_6(PO_4)_4$ oxyphosphate compound.

EXPERIMENTAL AND RESULTS

Preparation

Bi_2O_3 (Aldrich, 99.9%), CoO (Aldrich, 99%), and $(NH_4)_2HPO_4$ (Fluka, puriss) were mixed in a 1:2:1 molar ratio.

[1] Permanent address: Université Cadi Ayyad, Faculté des Sciences et Techniques, Department de Chimie et Environment, BP 523, Beni Mellal, Morocco.

[2] To whom correspondence should be addressed.

0022-4596/98 $25.00

The mixture was fused in a gold crucible at 950°C and slowly cooled at 3°C/h to room temperature. Three kinds of crystals were visually isolated from the inhomogeneous melt. Black octahedral crystals blocks were identified as Co_3O_4. Colorless plate-like crystals corresponding to the new $Bi_{6.67}P_4O_{20}$ compound are detailed in this work. Finally, purple needle-shaped crystals with the orthorombic unit cell [$a = 14.746(5)$ Å, b = 11.230(4) Å, c = 5.446(2) Å] are currently under investigation and will be described in a paper to come. Pure powder phases of $Bi_6M(PO_4)_4O_4$ ($M = Pb^{2+}, Sr^{2+}, Ca^{2+}, Cd^{2+}$) and $Bi_{6.5}A_{0.5}P_4O_{20}$ ($A = Li^+$, Na^+, K^+) were prepared by thermal treatment of stoichiometric mixtures of Bi_2O_3, $(NH_4)_2HPO_4$, and the corresponding oxide (Pb or Cd, Johnson Matthey, 99.9%) or carbonate (alkaline earths and alkali-Prolabo, rectapur). The preparations were performed in two steps. Reagents were first progressively heated from 300 to 500°C within 10 h to evacuate volatile species. The samples were then kept at 800°C for 48 h and quenched to room temperature. Samples were controlled by the powder X-ray diffraction method, and unit cell parameters were least-squares-refined using the data obtained with a Siemens D-5000 diffractometer equipped with a graphite crystal diffracted-beam monochromator and Cu$K\alpha$ radiation. Energy-dispersive spectroscopy (EDS) microprobe elemental analysis was performed on single crystals with a Philips 525M scanning electron microscope connected to an Edax PV9900 analyzer.

Single-Crystal X-Ray Analysis

A colorless plate-like single cystal was mounted on a glass fiber and exposed to X rays. Its unit cell is triclinic with parameters $a = 9.195(15)$ Å, b = 7.552(5) Å, c = 6.933(4) Å, $\alpha = 112.2(1)^\circ$, $\beta = 93.9(1)^\circ$, and $\gamma = 106.9(1)^\circ$. Data collection was performed on half of the reciprocal space using a Philips PW 1100 automated four-circle diffractometer using the conditions given in Table 1. For crystal refinement, the intensity of each reflection was corrected for background and for Lorentz and polarization effects. The absorption corrections were applied using the analytical method of De Meulenaer and Tompa (13) with, in the last stages of the structure determination, the true value of the linear absorption coefficients calculated from the final $Bi_{6.67}P_4O_{20}$ formula.

The structure determination was satisfactorily achieved in the $P\bar{1}$ space group with final reliability factors $R = 0.049$ and $R_w = 0.060$. First, four independent bismuth atoms were located using both the Patterson function calculation and SHELXS 86 software, (14). At this stage, the bismuth atom labeled Bi(4) fully occupies the 1(*a*) special position. Then, 2 phosphorus and 10 oxygen atoms were subsequently located by calculation of the Fourier difference synthesis. The use of all atomic positional and isotropic displacement parameters in the refinement process yielded $R = 0.105$ and $R_w = 0.113$. Nevertheless, the Bi(4) isotropic displacement parameter is abnormally high, 5.04 Å^2, as compared with the other Bi atoms. Therefore its occupancy was refined and perfectly converged to the 0.67(6) value, leading to the $Bi_{6.67}P_4O_{20}$ formula and involving a unique III valency state for all the bismuth atoms. In the last cycles of the refinement, the atomic positional parameters, anisotropic displacements for Bi and P atoms (Table 2), and improvement of absorption corrections yielded the final $R = 0.049$ and $R_w = 0.060$. The atomic scattering factors for neutral atoms were taken from "International Tables for X-Ray Crystallography" (15) and the values for the anomalous dispersion correction from Cromer and Liberman (16). The full-matrix least-squares refinement was performed with a local modification of the SFLS-5 program (17).

TABLE 1
Crystal Data: Intensity Measurement and Structure Refinement Parameters for $Bi_{6.67}(PO_4)O_4$ Single Crystal

Crystal Data	
Crystal symmetry	Triclinic
Space group	$P\bar{1}$
Cell dimension (Å)	$a = 9.195(15)$, $b = 7.552(5)$, $c = 6.933(4)$, $\alpha = 112.2(1)^\circ$, $\beta = 93.9(1)^\circ$, $\gamma = 106.9(1)^\circ$
Volume	417.9 Å^3
Z	1
Data collection	
Equipment	Philips PW 1100
λ (Mo$K\alpha$ (graphite monochromotor))	0.7107 Å
Scan mode	ω–2θ
Scan width (°)	1.5
θ range (°)	2–35
Standard reflections measured every 2 h (no decay)	201, $\bar{1}\bar{1}2$, $2\bar{2}2$
Recording reciprocal space	$-14 \le h \le 14$, $-12 \le k \le 12$, $0 \le l \le 10$
Number of measured reflections	3710
Number of reflections $I > 3\sigma(I)$	2804
Number of independent reflections	2624
μ(cm^{-1}) (for λ $K\alpha = 0.7107$ Å)	663
Limiting faces and distances (cm) from an arbitrary origin	102 $\bar{1}0\bar{2}$, 0.0041 $2\bar{1}1$ $\bar{2}1\bar{1}$, 0.0085 130 $\bar{1}\bar{3}0$, 0.0075 021, 0.00115
Transmission factor range	0.04–0.41
Refinement	
Number of refined parameters	94
$R = \sum[\|F_o\| - \|F_c\|]/\sum\|F_o\|$	0.049
$R_w = [\sum w(\|F_o\| - \|F_c\|)^2/\sum wF_o^2]^{1/2}$ with $w = 1/\sigma(F_o)$	0.060

TABLE 2
Positional and Isotropic (or Equivalent) or Anisotropic Thermal Parameters for $Bi_{6.67}(PO_4)_4O_4$

Atom	Site	Occupancy	x	y	z	B or B_{eq} (Å^2)
Bi(1)	2*i*	1	0.32601(6)	0.30422(8)	0.80927(7)	0.74(1)
Bi(2)	2*i*	1	0.08525(7)	0.78550(9)	0.43436(9)	1.26(1)
Bi(3)	2*i*	1	0.50979(6)	0.12976(8)	0.33518(7)	0.70(1)
Bi(4)	1*a*	0.67(6)	0	0	0	3.44(6)
P(1)	2*i*	1	0.7614(4)	0.2674(5)	0.0513(5)	0.54(8)
P(2)	2*i*	1	0.7466(4)	0.6059(5)	0.6580(5)	0.63(8)
O(1)	2*i*	1	0.855(2)	0.175(2)	−0.111(2)	1.2(1)
O(2)	2*i*	1	0.730(2)	0.752(2)	0.877(2)	1.2(1)
O(3)	2*i*	1	0.762(2)	0.182(2)	0.223(2)	0.9(1)
O(4)	2*i*	1	0.899(1)	0.908(2)	0.318(2)	0.8(1)
O(5)	2*i*	1	0.691(2)	0.389(2)	0.640(2)	1.1(1)
O(6)	2*i*	1	0.920(2)	0.682(2)	0.654(2)	1.4(1)
O(7)	2*i*	1	0.635(1)	0.970(2)	0.447(2)	0.6(1)
O(8)	2*i*	1	0.649(2)	0.621(2)	0.478(2)	1.0(1)
O(9)	2*i*	1	0.589(2)	0.206(2)	−0.051(2)	1.1(1)
O(10)	2*i*	1	0.837(7)	0.503(2)	0.149(2)	1.0(1)

Atom	U_{11}	U_{22}	U_{33}	U_{12}	U_{13}	U_{23}
Bi(1)	0.0091(2)	0.0089(2)	0.0086(2)	0.0021(2)	−0.0001(1)	0.0032(2)
Bi(2)	0.0193(3)	0.0114(2)	0.0191(2)	0.0072(2)	0.0082(2)	0.0061(2)
Bi(3)	0.0094(2)	0.0094(2)	0.0095(2)	0.0042(2)	0.0022(2)	0.0051(2)
Bi(4)	0.0346(10)	0.0139(7)	0.0628(13)	0.0078(6)	−0.0254(8)	0.0022(7)
P(1)	0.0073(14)	0.0064(14)	0.0071(12)	0.0025(11)	0.0029(10)	0.0028(11)
P(2)	0.0110(14)	0.0063(14)	0.0075(12)	0.0041(12)	0.0022(11)	0.0029(11)

TABLE 3
Selected Bond Distances (Å) and Angles (degrees) for $Bi_{6.67}(PO_4)_4O_4$

Bi(1) polyhedron		*sij*	Bi(3) polyhedron		*sij*
Bi(1)–O(2)$^{ii}_{112}$	2.429(13)	0.40	Bi(3)–O(3)	2.466(11)	0.37
Bi(1)–O(4)$^{ii}_{111}$	2.098(8)	0.99	Bi(3)–O(5)	2.357(9)	0.49
Bi(1)–O(7)$^{ii}_{111}$	2.308(10)	0.56	Bi(3)–O(7)$_{0\bar{1}0}$	2.184(13)	0.78
Bi(1)–O(8)$^{ii}_{111}$	2.277(12)	0.61	Bi(3)–O(7)$^{ii}_{111}$	2.275(11)	0.61
Bi(1)–O(9)$_{001}$	2.939(14)	0.10	Bi(3)–O(8)$^{ii}_{111}$	2.716(12)	0.19
Bi(1)–O(10)$^{ii}_{111}$	2.337(13)	0.52	Bi(3)–O(9)$^{ii}_{100}$	2.404(10)	0.43
⟨Bi(1)–O⟩	2.398	$\sum sij =$ 3.18	⟨Bi(3)–O⟩	2.400	$\sum sij =$ 2.87

Bi(2) polyhedron		*sij*	Bi(4) polyhedron		*sij*
Bi(2)–O(1)$^{ii}_{110}$	2.451(12)	0.38	Bi(4)–O(1)$_{100}$	2.404(15)	0.43
Bi(2)–O(3)$^{ii}_{111}$	2.567(11)	0.28	Bi(4)–O(2)$^{ii}_{100}$	2.404(15)	0.43
Bi(2)–O(4)$_{\bar{1}00}$	2.392(13)	0.45	Bi(4)–O(2)$_{\bar{1}\bar{1}\bar{1}}$	2.492(10)	0.34
Bi(2)–O(4)$^{ii}_{121}$	2.256(10)	0.65	Bi(4)–O(2)$^{ii}_{111}$	2.492(10)	0.34
Bi(2)–O(5)$^{ii}_{111}$	2.728(14)	0.18	Bi(4)–O(4)$_{\bar{1}\bar{1}0}$	2.696(12)	0.20
Bi(2)–O(6)$_{\bar{1}00}$	2.398(13)	0.44	Bi(4)–O(4)$^{ii}_{110}$	2.696(12)	0.20
Bi(2)–O(7)$^{ii}_{121}$	2.550(9)	0.29	Bi(4)–O(6)$_{\bar{1}\bar{1}\bar{1}}$	2.537(10)	0.30
Bi(2)–O(10)$_{100}$	2.650(8)	0.22	Bi(4)–O(6)$^{ii}_{111}$	2.537(10)	0.30
⟨Bi(2)–O⟩	2.499	$\sum sij =$ 2.89	⟨Bi(4)–O⟩	2.532	$\sum sij =$ 2.54

P(1) tetrahedron		*sij*	Angles	
P(1)–O(1)	1.539(12)	1.23	O(1)–P(1)–O(3)	109(2)°
P(1)–O(3)	1.552(14)	1.19	O(1)–P(1)–O(9)	113(2)°
P(1)–O(9)	1.549(12)	1.20	O(1)–P(1)–O(10)	109(1)°
P(1)–O(10)	1.555(11)	1.18	O(3)–P(1)–O(9)	106(1)°
			O(3)–P(1)–O(10)	112(2)°
			O(9)–P(1)–O(10)	109(1)°
⟨P(1)–O⟩	1.548	$\sum sij =$ 4.80	⟨O–P(1)–O⟩	109.7°

P(2) tetrahedron		*sij*	Angles	
P(2)–O(2)	1.555(11)	1.18	O(2)–P(2)–O(5)	110(2)°
P(2)–O(5)	1.521(14)	1.30	O(2)–P(2)–O(6)	105(1)°
P(2)–O(6)	1.537(13)	1.24	O(2)–P(2)–O(8)	109(1)°
P(2)–O(8)	1.543(13)	1.22	O(5)–P(2)–O(6)	112(2)°
			O(5)–P(2)–O(8)	110(2)°
			O(6)–P(2)–O(8)	110(2)°
⟨P(2)–O⟩	1.539	$\sum sij =$ 4.94	⟨O–P(2)–O⟩	109.3°

[a] *ii* is given for the $-x, -y, -z$ position.

DISCUSSION

Structure Description

Selected bond distances, angles, and bond valence sums calculated using Brown and Altermatt's data (18) are given in Table 3. Taking into account the Bi–O bonds shorter than 3 Å, Bi(1) and Bi(3) oxygen polyhedra consist of six atoms forming strongly distorted octahedra (Fig. 1), whereas the coordination number for Bi(2) and Bi(4) is 8. The low-symmetry environment is usual for Bi^{3+} cations and is in fact to be completed by the $6s^2$ stereoactive lone-pair *E*. This effect is especially pointed out around Bi(1) which is coordinated by four shortly bonded oxygen atoms [O(4), O(7), O(8) and O(10)] at the same side, $2.098 < \text{Bi–O} < 2.337$, whereas O(9) and O(2) are longly bonded at the other side which would host E. Such coordination is common for the Bi^{3+} cation, as for instance in sillen-type oxyhalides (19) and in the Aurivillius series (20). It was also observed in most of the independent Bi atoms of the recently characterized $Bi_9V_2ClO_{18}$ (21). One indeed observes for Bi(3) a BiO_3 pyramid characterized by three short Bi–O distances ranging from 2.27 to 2.35 Å. The same distance considerations applied to Bi(3) would set the lone pair oriented toward the center of the O(8)–O(9)–O(3) triangle, leading to a BiO_3E tetrahedral coordination. This phenomenon was noted in the $Bi_{2+x}Sr_{3-x}Fe_2O_{9+\delta}$ compounds (22) related to the well-known bismuth–copper superconducting oxides, but was also evidenced in the above-reported $Bi_9V_2ClO_{18}$ (21). The Bi(2) environment is most obstructed but the large available space released in the O(5)–Bi–O(10) plane is attractive for the lone-pair location. Astonishingly, Bi(4) occupies a symmetry center but its high displacement factor, $B = 3.44$ Å, would allow a slight displacement from the $\bar{1}$ origin. In such a case, the average superposition of two symmetrically related [atom + lone pair] positions would exaggerate the thermal motion of this cation. The partial occupancy of its crystallographic site also contributes to increase the thermal parameter. In fact, the low value of the bond valence sum calculation for Bi(4), 2.54, most likely favors an effective split at both sides to its central position that would significantly increase the $\sum S_{ij}$ value. However,

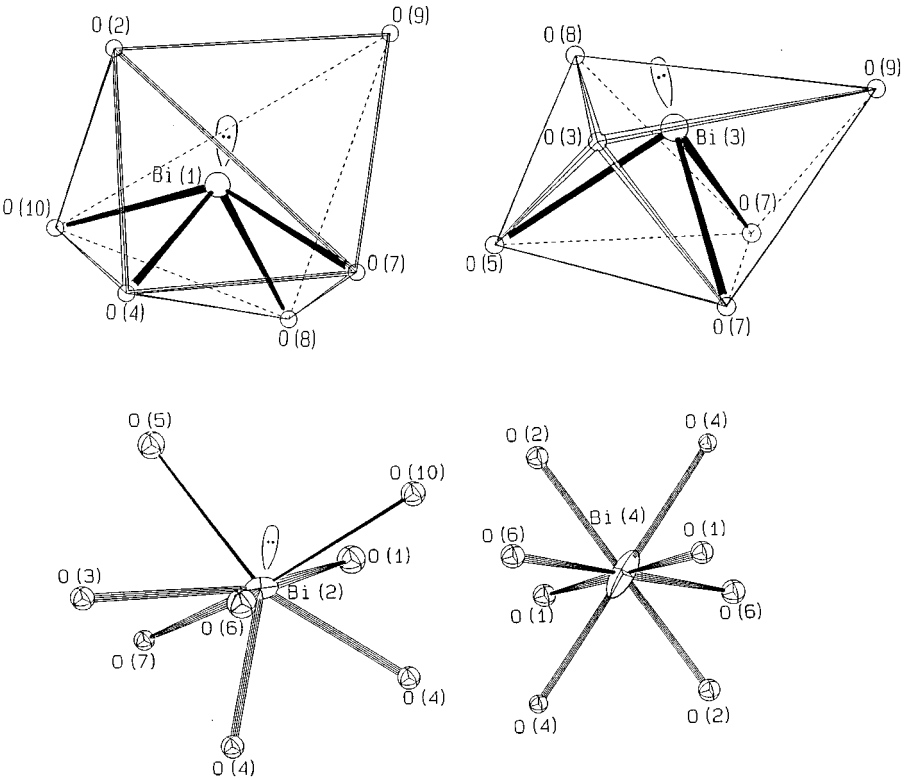

FIG. 1. The four bismuth polyhedra and assumed lone pair location for strongly distorted Bi(1), Bi(2), and Bi(3) environments.

attempts to split Bi(4) in a general position did not improve the refinement convergence. Figure 1 represents both oxygen coordination polyhedra of the four independent bismuth atoms.

P(1) and P(2) atoms both occupy the central interstices of regular tetrahedra with P–O distances included in the ranges 1.539(12)–1.555(11) and 1.521(14)–1.555(11) Å, respectively.

Bi(1)–O(9) being 2.939(14) Å, it was voluntarily removed from the Bi(1) environment in the polyhedra linkage consideration to allow the clearest description. Then, the $Bi_{6.67}(PO_4)_4O_4$ framework is formed by assembling BiO_5, BiO_6, BiO_8, and PO_4 polyhedra. A $Bi(3)O_6$ octahedron shares the O(7)–O(8) edge with a $Bi(1)O_5$ polyhedron and the O(3)–O(5)–O(7) face with a $Bi(2)O_8$ polyhedron to form the trimeric building unit of the structure (Fig. 2). The translation of the unit along *a* leads to infinite chains of bismuth oxygen polyhedra with the sequence Bi(1)–Bi(3)–Bi(2)–. Two chains related by a symmetry center are connected by O(4) and O(7) atoms to constitute infinite ribbons parallel to the *a* axis. Two $Bi(3)O_6$ octahedra are associated via a common O(7)–O(7) edge, whereas one $Bi(1)O_5$ polyhedron shares an O(4)–O(7) edge with a $Bi(2)O_8$ entity. Thus, two symmetrically related ribbons are connected by the Bi(4) polyhedra located around the center of inversion. It shares its two opposite O(1)–O(2)–O(4) faces with one $Bi(1)Bi(2)O_{11}$ dimer of each ribbon and two O(2)–O(4) edges with neighboring $Bi(2)O_8$ polyhedra (Fig. 3), leading to complex infinite slabs of formula $(Bi_{6.67}O_{20})_\infty^{20-}$, considering the Bi(4) partial occupancy, parallel to the (*ac*) plane. It sounds attractive to describe the bismuth polyhedra connection considering only the bridging O(4) and O(7) atoms. Thus, Fig. 4 clearly evidences the ensuing $(Bi_{6.67}O_4)_\infty^{12+}$ slabs. These slabs can be described as tetrameric units formed by four Bi_4O tetrahedra connected by opposite Bi–Bi edges. These tetrameric units are then linked by Bi(2)–Bi(2) edges to form ribbons parallel to *a*. These ribbons share Bi(4) corners. Finally, the cohesion between these layers is executed through PO_4^{3-} tetrahedra. $P(1)O_4$ and $P(2)O_4$ have a balanced role, sharing three for the former (one for the latter) and one (three) oxygen corner with the averaged $y = 0$ and $y = 1$ sheets, respectively, as shown in Fig. 2.

Thermal Stability of Phases

The calculated X-ray pattern for $Bi_{6.67}P_4O_{20}$ corresponds to the $2Bi_2O_3$–$7BiPO_4$ compound stable beyond 910°C evidenced during the Bi_2O_3–$BiPO_4$ phase diagram investigation (1). It is noteworthy that a previous work on this system did not show evidence of a peculiar behavior at

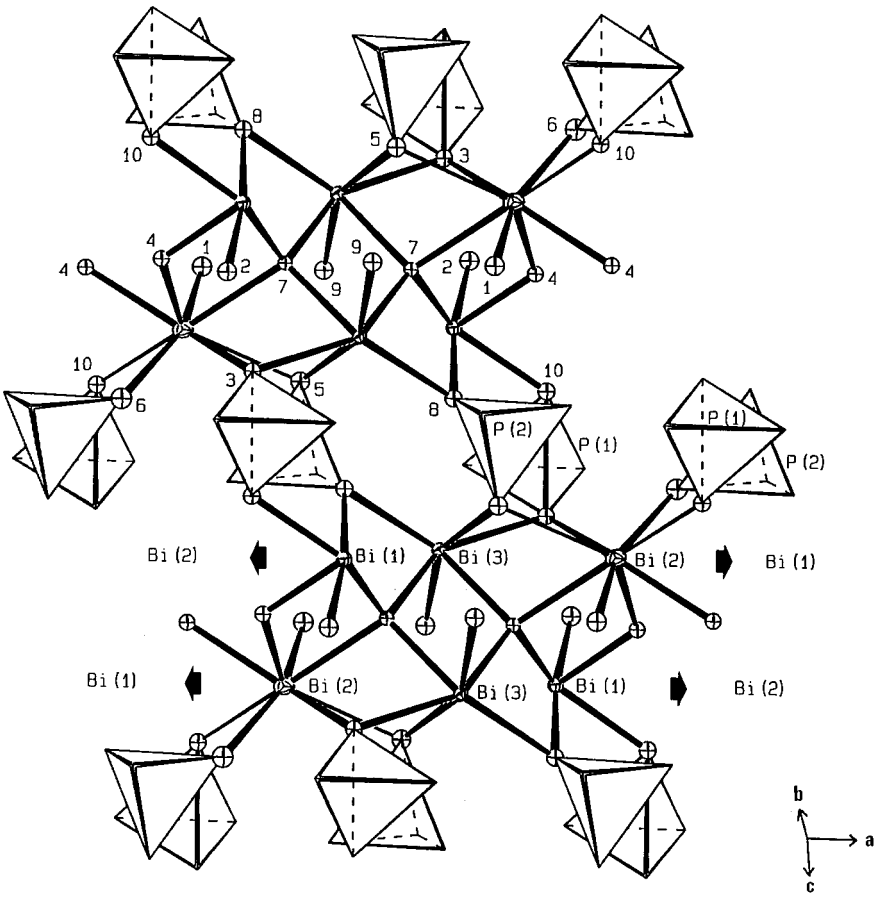

FIG. 2. The –Bi(2)Bi(1)–Bi(3)2–Bi(1)Bi(2)– chain elementary motif connected by PO_4 tetrahedra.

this composition (2). The compound melts incongruently and give rise to mixture of $BiPO_4$ and $3Bi_2O_3$–$8BiPO_4$ on cooling. The most likely $Bi_{6.67}P_4O_{20}$ stoichiometry is, actually, very close to the latter domain and can be noted as $2Bi_2O_3$–$6BiPO_4$. It would have been room temperature stabilized by cobalt traces from the starting charge. However, the transparent appearance of the single crystals obtained does not favor the presence of a transition metal. In addition, cobalt was not detected by EDS microprobe elemental and semiquantitative analysis performed on single crystals. The measurement indicated a Bi/P ratio of 1.72, close to the formal value of 1.66 for the $Bi_{6.67}P_4O_{20}$ formula. We must therefore conclude that single crystals do not grow without cobalt, which would behave as a mineralizer. Moreover, attempts to quench $Bi_{6.67}P_4O_{20}$ from 950°C to room temperature using liquid nitrogen were not successful.

Mixed Cation Compounds

By distinguishing the partially occupied Bi(4) atom, the formula of the studied compound can be written $Bi_{2/3}Bi_6(PO_4)_4O_4$. This consideration leads to the attractive possibility of substitution of one M^{2+} cation for $\frac{2}{3}Bi^{3+}$ or $0.5A^{+}$ cation for $\frac{1}{6}Bi^{3+}$, yielding respectively $Bi_6MP_4O_{20}$ (M = Sr^{2+}, Cd^{2+}, Ca^{2+}, Pb^{2+}) and $Bi_{6.5}A_{0.5}P_4O_{20}$ (A =

TABLE 4
Unit Cell Parameters Versus the Ionic Radius (Å) (VIII Coordination) of the Substituting Element

Compound	Ionic Radius	a(Å)	b(Å)	c(Å)	α(°)	β(°)	γ(°)
$Bi_{6.5}Li_{0.5}P_4O_{20}$ $F_{20} = 71(0.0061, 46)$	0.92	9.214(2)	7.576(2)	6.976(2)	112.03(1)	93.56(1)	107.20(1)
$Bi_{6.5}Na_{0.5}P_4O_{20}$ $F_{20} = 108(0.0039, 46)$	1.18	9.203(2)	7.540(2)	6.921(1)	112.23(1)	93.64(1)	107.07(1)
$Bi_{6.5}K_{0.5}P_4O_{20}$ $F_{20} = 94(0.0046, 46)$	1.51	9.198(2)	7.564(2)	6.963(2)	111.97(1)	93.40(1)	107.24(1)
$Bi_6SrP_4O_{20}$ $F_{20} = 52(0.0084, 46)$	1.26	9.210(2)	7.523(2)	6.906(2)	112.42(1)	93.68(1)	107.00(1)
$Bi_6CdP_4O_{20}$ $F_{20} = 53(0.0082, 46)$	1.10	9.188(4)	7.513(2)	6.894(2)	112.03(1)	94.24(1)	106.81(2)
$Bi_6CaP_4O_{20}$ $F_{20} = 52(0.0085, 46)$	1.12	9.195(2)	7.540(2)	6.913(2)	112.19(1)	93.85(1)	107.10(2)
$Bi_6PbP_4O_{20}$ $F_{20} = 57(0.0076, 46)$	1.29	9.226(2)	7.584(2)	6.995(2)	112.04(1)	93.46(1)	107.25(2)

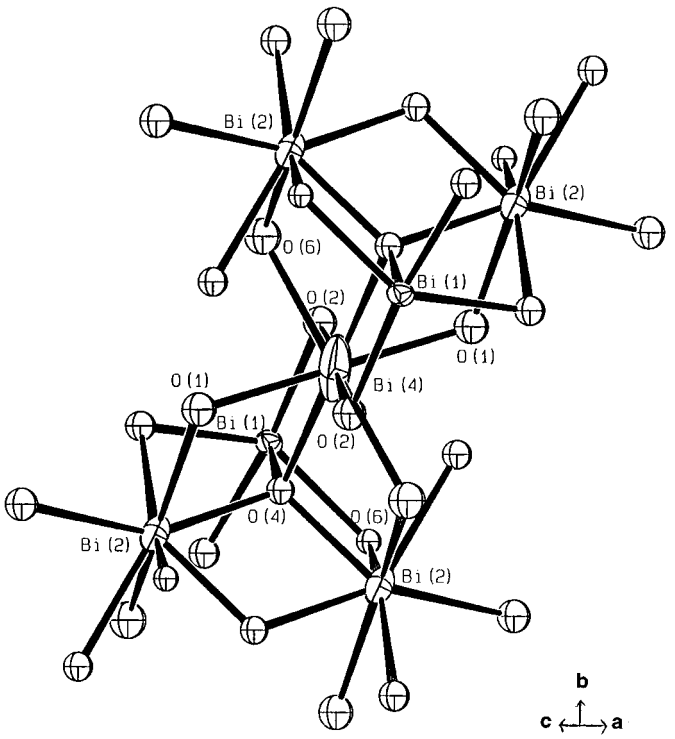

FIG. 3. Two chains connected via $Bi(4)O_8$.

Li^+, Na^+, K^+). They all led to pure polycrystalline materials isostructural with $Bi_{6.67}P_4O_{20}$, supporting the substituting room temperature stabilization concept described above and the nonactive $6s^2$ lone pair for the Bi(4) ion. This involves for the second series mixed occupancy of the 1(*a*) site by both Bi^{3+} and the alkali element. X-ray powder diffraction patterns did not reveal superstructure peaks for the considered samples; nevertheless, single-crystal studies are needed to conclude to the possible existence of a cationic ordering between the two kinds of hosts. Table 4 shows the least-squares-refined unit cell parameters versus the different cation ionic radii accompanied with their figures of merit, as defined by Smith and Synder, which indicate the completeness and accuracy of measured interplanar spacings (23). The cell is slightly changed with the doping agent nature. Each case must be treated on its own merits and no obvious rule can be pointed out. We therefore note that the smallest *a*, *b*, and *c* parameters of the $Bi_6M(PO_4)_4O_4$ series are obtained for $M = Cd^{2+}$, which possesses the smallest

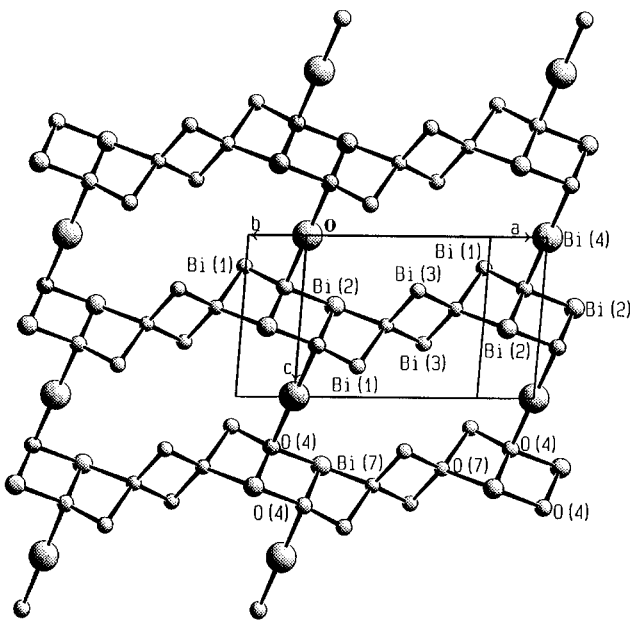

FIG. 4. $(Bi_{6.67}O_4)_\infty^{1,2+}$ slabs in the (*ac*) plane.

TABLE 5
Refined Powder Pattern for $PbBi_6(PO_4)_4O_4$

hkl	d_{obs}(Å)	d_{cal}(Å)	I/I_0
010	6.60	6.59	25.1
001	6.36	6.36	9.1
$01\bar{1}$	5.97	5.97	12.8
$10\bar{1}$	5.67	5.67	5.4
$1\bar{1}1$	5.24	5.24	5.1
101	4.71	4.71	7.6
200	4.32	4.32	9.4
$1\bar{1}\bar{1}$	4.031	4.030	31.3
$2\bar{1}1$	3.741	3.740	16.5
$02\bar{1}$	3.598	3.597	27.4
$1\bar{2}0$	3.513	3.512	10.2
020	3.295	3.299	37.2
201		3.291	
$11\bar{2}$	3.263	3.263	100
$2\bar{2}1$	3.219	3.219	71.5
210	3.152	3.152	67.0
$3\bar{1}0$	3.056	3.055	16.1
$30\bar{1}$	2.840	2.840	8.3
102	2.813	2.813	33.3
$3\bar{1}\bar{1}$	2.770	2.770	47.5
$1\bar{2}\bar{1}$	2.692	2.692	41.4
$2\bar{2}2$	2.620	2.621	17.4
$1\bar{1}\bar{2}$	2.597	2.597	5.2
211	2.506	2.506	3.8
$31\bar{1}$	2.473	2.472	8.4
$03\bar{1}$	2.408	2.408	19.3
$4\bar{1}0$	2.303	2.302	7.8
$2\bar{3}2$	2.254	2.254	10.4
121	2.234	2.233	12.9
$1\bar{1}3$	2.188	2.188	12.2
$3\bar{3}0$	2.141	2.140	23.0
$4\bar{1}1$	2.122	2.122	16.5
$20\bar{3}$	2.068	2.069	10.4
$1\bar{3}3$	1.998	1.998	16.5
$40\bar{2}$	1.974	1.974	10.3
$32\bar{2}$	1.951	1.951	16.8
$2\bar{1}3$	1.852	1.852	19.2
$4\bar{1}2$	1.811	1.812	13.2

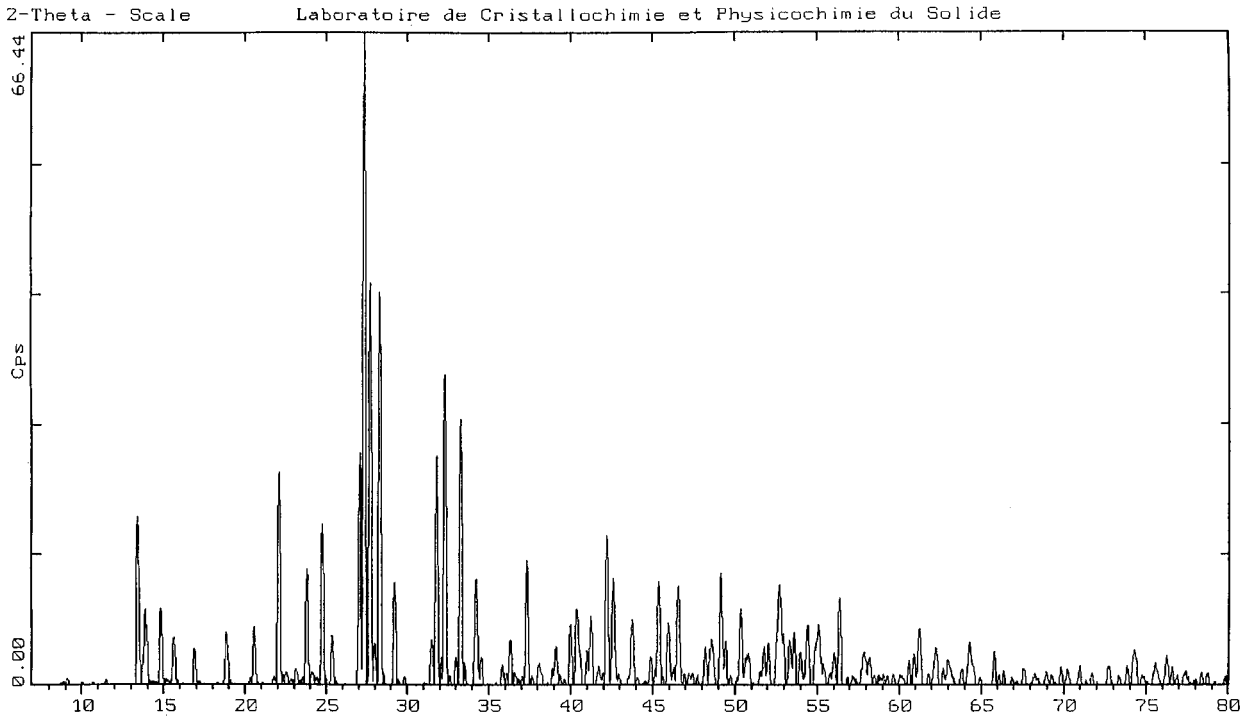

FIG. 5. X-ray pattern for $PbBi_6(PO_4)O_4$.

ionic radius. Astonishingly the volume of the Li phase (422.9 Å^3) is higher than that of the Na phase (416.6 Å^3). This surprising phenomenon was already observed in solids, for example, the alkali inserted tungsten bronze A_xWO_3 (24). The crystal structure study of substituted compounds, particularly $PbBi_6(PO_4)_4O_4$, which combines two lone pair cations, is in progress. Its refined X-ray pattern is presented in Table 5 and Fig. 5. Astonishingly, during investigation of the Bi_2O_3–$BiVO_4$ system (25, 26), no homologous compound of stoichiometry $Bi_{6.67}(VO_4)_4O_4$ was detected. However, it appears of interest to synthesize $M^{2+}Bi_6(VO_4)_4O_4$ materials.

REFERENCES

1. J. P. Wignacourt, M. Drache, P. Conflant, and J. C. Boivin, *J. Chim. Phys.* **88,** 1933 (1991).
2. V. V. Volkov, L. A. Zhereb, Yu. F. Kargin, V. M. Skorikov, and I. V. Tanaev, *Russ. J. Inorg. Chem.* **28,** 1002 (1983).
3. A. Watanabe, H. Komada, and S. Takenouchi, *J. Solid State Chem.* **85,** 85, 76 (1990).
4. J. P. Wignacourt, M. Drache, P. Conflant, and J. C. Boivin, *J. Chim. Phys.* **88,** 1939 (1991).
5. J. P. Wignacourt, M. Drache, and P. Conflant, *J. Solid State Chem.* **85,** 76 (1990).
6. F. Abraham, M. F. Debreuille-Gresse, G. Mairesse, and G. Nowogrocki, *Solid State Ionics* **28–30,** 529 (1988).
7. F. Abraham, J. C. Boivin, G. Mairesse, and G. Nowogrocki, *Solid State Ionics* **40/41,** 934 (1990).
8. G. Mairesse, *in* "Fast Ion Transport in Solids" (B. Scorsati, Ed.), p. 271, Kluwer, Dordrecht, 1993.
9. J. R. Dygas, P. Kurek, and M. W. Breiter, *Electrochim. Acta* **40,** 1545 (1995).
10. F. Krok, I. Abrahams, D. Bangobango, W. Bogusz, and J. A. G. Nelstrop, *Solid State Ionics* **86–88,** 261 (1996).
11. F. Abraham, M. Ketatni, and B. Mernari, *Adv. Mater. Res.* **1/2,** 223 (1994).
12. B. Serien-Verdonck, Ph.D. thesis, Lille, 1991.
13. J. De Meulenaer and H. Tompa, *Acta Crystallogr.* **19,** 1014 (1965).
14. G. M. Sheldrick, "SHELXS-86 User Guide." Crystallography Department, University of Göltinger, 1986.
15. "International Tables for X-ray Crystallography." Vol. IV. Kynoch Press, Birmingham, 1974.
16. D. T. Cromer and D. Liberman, *J. Chem. Phys.* **53,** 1891 (1970).
17. C. T. Prewitt, "SFLS-5, Report ORNL-TM 305." Oak Ridge National Laboratory, Oak Ridge, TN, 1966.
18. I. D. Brown and D. Altermatt, *Acta Crystallogr. Sect. B* **41,** 244 (1985).
19. L. Sillen, *Z. Anorg. Allgem. Chem.* **246,** 331 (1941).
20. B. Aurivillius, *Ark. Kemi* **1,** 463 (1949).
21. O. Mentre and F. Abraham, *J. Solid State Chem.* **136,** 34 (1998).
22. O. Perez, H. Leligny, D. Grebille, J. M. Grenêche, Ph. Labbé, D. Groult, and B. Raveau, *Phys. Rev. B* **55,** 1236 (1997).
23. G. S. Smith and R. J. Snyder, *J. Appl. Crystallogr.* **12,** 60 (1979).
24. P. Hagenmuller, *in* "Non-stoichiometric Compounds, Tungsten Bronzes, Vanadium Bronzes and Related Compounds" (D. J. Bevan and P. Hagenmuller, Eds.), Vol. 1. Pergamon Press, Oxford, 1973.
25. Y. N. Blinovskov and A. A. Fotiev, *Russ. J. Inorg. Chem.* **31** (1), 145 (1987).
26. W. Zhou, *J. Solid State Chem.* **87,** 44 (1990).